ELECTRONIC CONDUCTANCE OF MULTI-WALLED CARBON NANOTUBES HAVING RELIABLE ELECTRICAL CONTACTS

E. GRAUGNARD, R. REIFENBERGER
Purdue University, Dept. of Physics, W. Lafayette, IN 47907, U.S.A.

B. WALSH
Purdue University, Electrical and Computer Engineering, W. Lafayette, IN 47907, USA

P.J. DE PABLO
Dept. Física de la Materia Condensada, Universidad Autónoma de Madrid, 28049-Madrid, Spain

The fabrication and characterization of reliable electrical contacts to multi-walled carbon nanotubes is described. Using these contacts, electrical currents as high as a few mA can be passed through some multi-walled nanotubes without adverse consequences. This fabrication method results in low-resistance contacts to multi-walled carbon nanotubes and allows the acquisition of reproducible I(V) data between 300 K and 4.2 K.

1 Introduction

There is continuing interest in the electronic properties of carbon nanotubes.[1] From a scientific standpoint, carbon nanotubes represent a physical realization of a model one-dimensional (1D) electronic system. This has lead to many predictions for single wall nanotubes (SWNTs)[2,3,4,5,6,7,8,9,10,11,12,13,14,15] and multi-wall nanotubes (MWNTs).[7] A test of these theories often requires a measurement of the transport properties of a nanotube. A major problem in performing such experiments is the reliable attachment of current and voltage leads to nanotubes. Since the size mis-match between the nanotube diameter and contacting electrodes is considerable, a variety of innovative techniques have been proposed. As a result, transport data on SWNTs[16,17,18,19,20,21,22] and MWNTs[21,23,24,25,26,27,28,29,30] have been reported. Much of this prior work relies on a serendipitous deposition of nanotubes across contacts, the exposure of a nanotube to high energy electron or ion beams, and/or coating the nanotube with lithographic chemicals. All of these factors conspire to either limit the yield of useful samples or cause unwanted structural damage or modification to the nanotube under study. What is needed is a simple approach that does not suffer from these limitations.

To address this important issue, we have recently developed a technique

to make reliable electrical contacts to carbon nanotubes.[28] The technique is relatively simple and does not require sophisticated equipment to implement. In what follows, we report further studies designed to better characterize both the MWNTs and the electrical contacts to them.

2 Sample Preparation

An individual MWNT or a rope of a few MWNTs is selected from a nanotube boule using a darkfield microscope.[31] This selection is facilitated by contacting a MWNT in the boule with an etched Pt field emission tip. The end of the MWNT sticking out from the boule is opened by touching it with a Pt tip held at 15V with respect to the boule. After reducing the potential on the tip to 0V, a length of the protruding tube is brought into contact with the tip. After contact, a bias of about 5V is applied and, as the Pt tip is withdrawn from the MWNT boule, we find that a 5-10 μm long rope of MWNTs becomes attached to the tip and eventually breaks free from the boule. TEM studies show that both ends of the MWNT rope are opened during this procedure (see Fig. 1). The end of the MWNT that first makes contact with the Pt tip is opened by the initial touch of the biased Pt tip. The second end of the MWNT is opened when the selected tube (or rope) is separated from the MWNT boule. In both cases a visible emission of light is often observed during this selection and separation procedure, implying the presence of a localized, intense electrical arc.

Using micro-positioners, the MWNT attached to the Pt tip can be precisely transferred to a smooth glass substrate. A suitable shadow mask is then aligned perpendicular to the axis of the MWNT to shield the middle section of the nanotube during subsequent thin film evaporation. This procedure allows the ends of the MWNT to be covered with metal contact pads evaporated from metals of choice. An inexpensive shadow mask suitable for this purpose is made from commercially available 4.3 μm diam. tungsten wire.

The entire sample (MWNT, shadow mask and glass substrate) is then inserted into a multi-source e-beam evaporator. We typically evaporate a $\sim$10 nm thick Ti adhesion layer followed by $\sim$150 nm of Au. Following evaporation, a reliable electrical contact results beneath the ends of the MWNT which are now buried under a layer of metal. An advantage of this shadow-mask technique is that no chemical processing of the nanotube is required. Once the contact pads have been deposited, the sample can be inserted into an air scanning force microscope (SFM) and imaged using a variety of non-contact techniques. From the resulting images, it is usually clear which samples have survived the handling while transferring the samples into and out of the

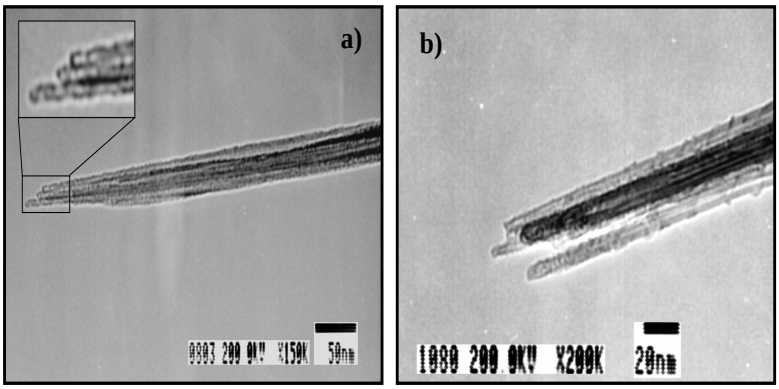

Figure 1: TEM images of the end-forms of typical MWNTs used in this study. In (a) the outer diameter of the MWNT rope is ∼50 nm. The inset is an enlarged view of the end of the rope, showing the presence of three MWNTs. In (b), another MWNT rope having an outer diameter near ∼40 nm is shown. Close examination of this image shows 5-6 MWNTs, each with a diameter of ∼ 7 nm.

evaporation chamber.

During the past year, about 80 samples were prepared following this procedure. Of these 80 samples, roughly 20 were deemed unacceptable after being fitted with a shadow mask and inspected in the dark field microscope. The 60 samples that passed this initial inspection were inserted into the evaporator and processed to produce contact pads. Of these 60, about 20 were found to be electrically continuous, thus allowing the acquisition of electronic transport data.

SFM images of two samples are illustrated in Fig. 2 (a) and (b). In Fig. 2 (a), we show a SFM image of an electrically continuous sample with two evaporated Ti/Au contact pads covering the ends of a MWNT. A common failure mode for the nanotubes appears to be an electrostatic discharge which evidently causes a high current to pass through the nanotube. An example of this failure mode is illustrated in Fig. 2 (b) which shows a nanotube that has been completely destroyed. Evidence for a local melting of the Ti/Au contacts is clear. Since bulk Au melts near $\sim 1000^o$ C, the local melting of the Au contact pad provides evidence of a high temperature rise in the vicinity of the MWNT/contact junction just prior to the destruction of the MWNT.

TEM studies (see Fig. 1) suggests that a typical MWNT sample is comprised of a few individual MWNTs. Further evidence supporting this view is given in Fig. 3 (a) and (b) which illustrates how individual MWNTs inter-

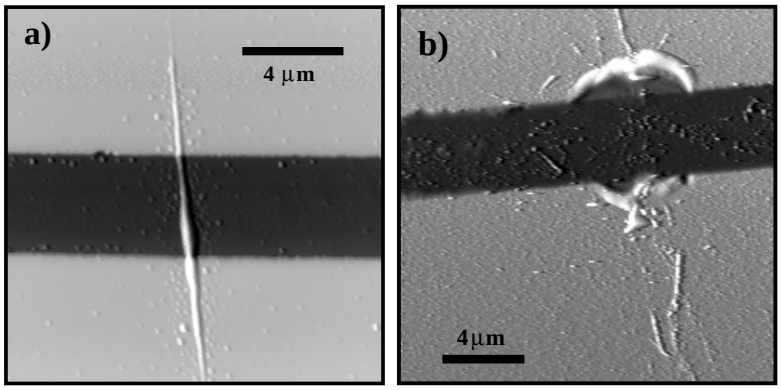

Figure 2: In (a), a non-contact SFM image of a typical MWNT sample, No. 40. The image shows a MWNT crossing a 4.3 μm wide trench. The two evaporated Ti/Au contact pads lie on top of the ends of the nanotube. In (b), a non-contact SFM image of MWNT sample No. 5 that has been blown apart, presumably by an electrostatic discharge. Remnants of the MWNT are found scattered throughout the image. In addition, what appears to be a local melting of the Ti/Au contact pads is evident.

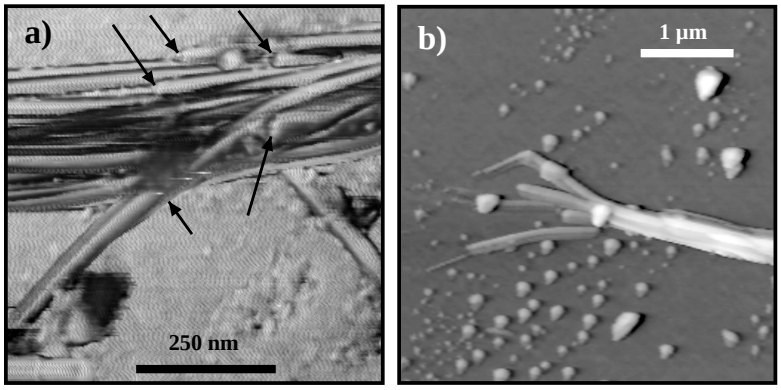

Figure 3: In (a), a SFM phase contrast image of sample No. 25 showing multiple nanotubes in a MWNT rope. This image was taken near the middle of the MWNT sample and reveals the ends of several MWNTs (see arrows), suggesting that only a few MWNTs remain electrically continuous across the entire 4.3 μm distance between the two contact pads. In (b), a SFM image of sample No. 49 showing the individual MWNTs unraveling at the end of the rope. The diameters of the individual MWNTs in both images are distorted (enlarged) due to tip dilation effects.

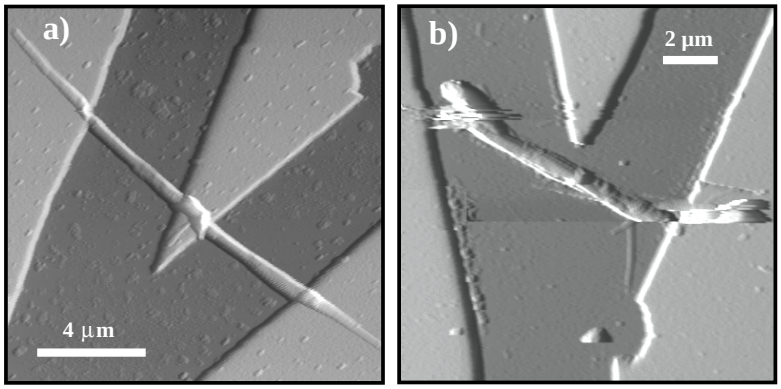

Figure 4: Using a two-wire shadow-mask technique, it is possible to define a third electrode in close proximity to the two contact pads. In (a), the third electrode makes electrical contact to the middle of MWNT sample No. 66. In (b), the third electrode acts as a nearby gate. The MWNT (sample No. 68) shown in (b) failed to make an electrical connection to the left contact pad.

twine in our samples. Fig. 3 (a) is a phase contrast SFM image taken near the center of a mounted MWNT. The phase imaging mode is used to enhance contrast.[32,33,34] This image provides clear evidence that broken MWNTs exist along the length of the rope. Fig. 3 (b) shows individual MWNTs that have unraveled at the end of a MWNT rope. Based on these studies, it is likely that a few, perhaps only one, of the individual MWNTs in a rope remains continuous across the entire 4.3 μm length between the contact pads. Thus experimental transport measurements in our samples may be dominated by the electronic properties of only one MWNT. This view is consistent with our electrical transport data presented below.

One advantage of our procedure for making contacts to nanotubes is its flexibility. This is demonstrated in Fig. 4 which illustrates how a third electrode can be added about midway between the two contact pads. This was accomplished by carefully positioning two W wires so that they crossed above (and near the center of) the MWNT. In Fig. 4 (a), the third electrode makes electrical contact with the MWNT. Fig. 4 (b) illustrates how the third electrode can be used as a nearby electrostatic gate.

3 Conductance as a function of temperature

After preparing MWNT samples as described above, I(V) data were obtained using a quasi 4-terminal technique, where two wires are attached to each of

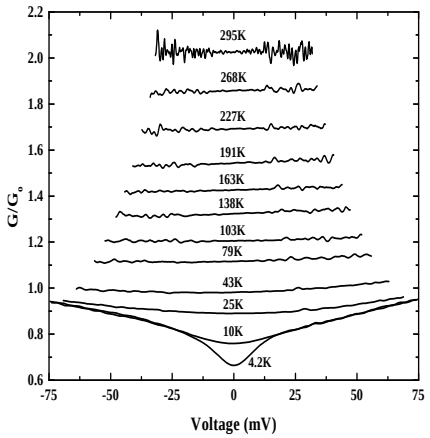

Figure 5: The conductance G(V,T) plotted in units of the quantum of conductance, $G_o = 2e^2/h$, as a function of applied bias voltage V for sample No. 66. The data are plotted at 12 different temperatures, with the temperature label adjacent to each data set. The conductance at room temperature is 2.0 G_o.

the two nanotube contact pads. Our data suggest that the resistance between the contact pad and the nanotube is typically less than 10kΩ.

Conductance data as a function of temperature were obtained by placing a MWNT sample on a brass mounting plate, attached to the end of a thin-walled stainless-steel tube. A silicon diode was thermally-anchored to the brass plate to measure temperature. Four electrical leads (two for current, two to measure voltage) were attached to the Ti/Au contact pads with a small amount of silver paint. The brass plate was inserted into a stainless-steel can and the entire assembly was evacuated to forepump pressures (< 5 Torr) before inserting into a liquid helium storage dewar. Carefully positioning the stainless-steel can with respect to the liquid He level within the dewar controlled the temperature of the mounting plate and allowed conductance measurements between room temperature and 4.2K. The samples prepared using the above procedure withstood repeated thermal cycling and yielded conductance values which were reproducible.

By measuring I(V) at different temperatures, it was possible to calculate the conductance of the MWNT sample (G(V,T) $\equiv$ dI/dV) as a function of both applied voltage and temperature. Resulting data are plotted in Fig. 5 and illustrate several important features. At room temperature the mean

conductance is nearly independent of applied bias voltage indicating ohmic behavior. Also evident in the conductance data near room temperature is a voltage and temperature dependent noise. At temperatures below ~20 K, a downward bow develops in G(V,T) and signals the gradual appearance of a non-linearity in I(V). This dip in G(V,T) evolves into a conductance gap which is clearly developed at temperatures near 4 K. Another interesting feature is the saturation of the conductance at higher bias for temperatures below ~20 K. These data are typical for all the samples we have studied to date. A complete theory of electronic conduction in carbon nanotubes must successfully address each of these features.

Acknowledgments

The authors would like to thank S. Datta, R.P. Andres and D. Janes for helpful conversations throughout the course of this work. The sample of MWNTs was kindly supplied by R. Smalley.

References

1. M.S. Dresselhaus, G. Dresselhaus, and P.C. Eklund, *Science of Fullerenes and Carbon Nanotubes*, Academic Press, New York, 1996.
2. J.W. Mintmire, B.I. Dunlap, and C.T. White, Phys. Rev. Lett. **1992**, 631 (1992).
3. W. Tian and S. Datta, Phys. Rev. **B49**, 5097 (1994).
4. M.F. Lin and K.W.-K. Shung, Phys. Rev. **B51**, 7592 (1995).
5. L. Chico, L.X. Benedict, S.G. Louie, and M.L. Cohen, Phys. Rev. **B54**, 2600 (1996).
6. C.L. Kane and E.J. Mele, Phys. Rev. Lett. **78**, 1932 (1997).
7. M.F. Lin, D.S. Chuu, and K.W.-K. Shung, Phys. Rev. **B56**, 1430 (1997).
8. O.M. Yevtushenko, G.Ya. Slepyan, S.A. Maksimenko, A. Lakhtakia, and D.A. Romanov, Phys. Rev. Lett. **79**, 1102 (1997).
9. R. Egger and A.O. Gogolin, Phys. Rev. Lett. **79**, 5082 (1997).
10. C. Kane, L. Balents, and M.P.A. Fisher, Phys. Rev. Lett. **79**, 5086 (1997).
11. C.T. White and T.N. Todorov, Nature **393**, 240 (1998).
12. C.T. White and J.W. Mintmire, Nature **394**, 29 (1998).
13. M.P. Anantram, J. Han, and T.R. Govindan, in *Molecular Elctronics: Science and Technology*, edited by A. Aviram and M. Ratner, volume 852, New York Academy of Sciences, New York, NY, 1998.
14. K. Esfarjani, A.A. Farajian, Y. Hashi, and Y. Kawazoe, Appl. Phys. Lett. **74**, 79 (1999).

15. A.A. Farajian, K. Esfarjani, and Y. Kawazoe, Phys. Rev. Lett. **82**, 5084 (1999).
16. L. Langer, L. Stockman, J.P. Heremans, V. Bayot, C.H. Olk, C. Van Haesendonck, Y. Bruynseraede, and J-P. Issi, J. Mater. Res. **9**, 927 (1994).
17. S.J. Tans, M.H. Devoret, H. Dai, A. Thess, R.E. Smalley, L.J. Geerligs, and C. Dekker, Nature **386**, 474 (1997).
18. T. W. Odom, J. L. Huang, P. Kim, and C. M. Lieber, Nature **391**, 62 (1998).
19. Jeroen W. G. Wildöer, L. C. Venema, A. G. Rinzler, R. E. Smalley, and C. Dekker, Nature **391**, 59 (1998).
20. A. Bezryadin, R.M. Verschueren, S.J. Tans, and C. Dekker, Phys. Rev. Lett. **80**, 4036 (1998).
21. R. Martel, T. Schmidt, H.R. Shea, T. Hertel, and Ph. Avouris, Appl. Phys. Lett. **73**, 2447 (1998).
22. H.T. Soh, C.F. Quate, A.F. Morpurgo, C.M. Marcus, J. Kong, and H. Dai, Appl. Phys. Lett. **75**, 627 (1999).
23. L. Langer, V. Bayot, E. Grivei, J-P. Issi, J.P. Heremans, C.H. Olk, L. Stockman, C. Van Haesendonck, and Y. Bruynseraede, Phys. Rev. Lett. **76**, 479 (1996).
24. A.Yu. Kasumov, I.I. Khodos, P.M. Ajayan, and C. Colloex, Europhys. Lett. **34**, 429 (1996).
25. T.W. Ebbesen, H.J. Lezec, H. Hiura, J.W. Bennett, H.F. Ghaemi, and T. Thio, Nature **382**, 54 (1996).
26. S. Frank, P. Poncharel, Z.L. Wang, and W. A. de Heer, Science **20**, 1744 (1998).
27. A. Bachtold, M. Henny, C. Terrier, C. Strunk, C. Schönenberger, J.-P. Salvetat, J.-M. Bonard, and L. Forró, App. Phys. Lett. **73**, 274 (1998).
28. P.J. De Pablo, E. Graugnard, B. Walsh, R.P. Andres, S. Datta, and R. Reifenberger, Appl. Phys. Lett. **74**, 323 (1999).
29. A. Bachtold, C. Strunk, J-P. Salvetat, J-M. Bonard, L. Forró, T. Nussbaumer, and C. Schönenberger, Nature **397**, 673 (1999).
30. B. Wei, R. Spolenak, P. Kohler-Redlich, M. Rühle, and E. Arzt, Appl. Phys. Lett. **74**, 3149 (1999).
31. The process was observed using a Nikon Epiphot 200 darkfield microscope equipped with a 50X/0.55 objective having an overall magnification of 750X.
32. B. Anczykowski, D. Krüger, K.L. Babcock, and H. Fuchs, Ultramicroscopy **66**, 251 (1996).
33. J. Tamayo and R. García, Appl. Phys. Lett. **71**, 2394 (1997).

34. S.N. Magonov, V. Elings, and M.-H. Whangbo, Surf. Sci. **375**, 385 (1997).